Remote Sensing of Environment 128 (2013) 162–175

Contents lists available at SciVerse ScienceDirect

Remote Sensing of Environment

journal homepage: www.elsevier.com/locate/rse

Remote sensing of picophytoplankton distribution in the northern South China Sea

Xiaoju Pan [a,*], George T.F. Wong [a,b], Tung-Yuan Ho [a], Fuh-Kwo Shiah [a], Hongbin Liu [c]

[a] Research Center for Environmental Changes, Academia Sinica, Taipei, Taiwan
[b] Institute of Hydrological and Oceanic Sciences, National Central University, Jhongli, Taiwan
[c] Division of Life Science, and Division of Environment, Hong Kong University of Science and Technology, Clear Water Bay, Hong Kong, China

ARTICLE INFO

Article history:
Received 27 November 2011
Received in revised form 19 September 2012
Accepted 15 October 2012
Available online xxxx

Keywords:
Remote sensing
Picophytoplankton
Northern South China Sea
HPLC pigments
Phytoplankton composition
MODIS-Aqua

ABSTRACT

By using a global data set (NOMAD), improved algorithms were developed for deducing from ocean color remote sensing data the concentrations of phytoplankton pigments, total chlorophyll *a* (TChl_*a*), zeaxanthin (Zea) and fucoxanthin (Fuco), and the associated primary phytoplankton groups, namely, *Prochlorococcus*, *Synechococcus*, haptophytes and diatoms, in the oceans. A modified classification for the waters of the world's ocean based on the dominant phytoplankton group was then devised. By using a local data set from the northern South China Sea (NSCS), algorithms were also developed for assessing the cell abundances of picophytoplankton, *Prochlorococcus*, *Synechococcus* and pico-eukaryotes, in this region. These algorithms were then applied to the remotely sensed data from the MODerate-resolution Imaging Spectrometer at Aqua sensor (MODIS-Aqua) to study the abundances and the distributional patterns of picophytoplankton in the entire NSCS. The results agreed well with field observations, which were available only from selected locations in the study area. On a basin scale, the results were consistent with expected variations in phytoplankton pigments, phytoplankton community composition, and picophytoplankton biomass, in response to the major known environmental phenomena in the NSCS, such as the progressive increase in biological productivity towards the coast, the runoff from the Pearl River, higher biological productivity in the wintertime, upwelling around the Taiwan Bank, winter upwelling northwest of the Luzon Island, and the transformation and dissipation of internal waves off the Dongsha Atoll. This work represents the first effort in estimating the cell abundances of the principal picophytoplankton groups in the oceans from space. The general application of this approach to the global ocean needs to be further validated and calibrated with a more extensive data base from field observations in other parts of the oceans.

1. Introduction

Picophytoplankton (<2 μm), such as cyanobacteria and prochlorophytes, contribute significantly to phytoplankton biomass, primary production, carbon flux, and nutrient regeneration in the ocean, especially in the oligotrophic waters (Campbell & Vaulot, 1993; Campbell et al., 1994; Li et al., 1983; Liu et al., 2007). Their ability to capture nutrients efficiently and, in selected species such as *Trichococcus*, to fix nitrogen gives them a competitive advantage over other phytoplankton in oligotrophic waters (Campbell & Vaulot, 1993; Campbell et al., 1994; Li et al., 1983). Observations in the oligotrophic subtropical and tropical waters at the Hawaii Ocean Time-series station (ALOHA; 22.77° N, 158.09° W) and the SouthEast Asia Time-series Study station (SEATS; ~18° N, ~116° E) indicate that picophytoplankton can account for up to 80% of the phytoplankton biomass (Campbell & Vaulot, 1993; Liu et al., 2007).

Picophytoplankton are traditionally assessed in discrete water samples by microscopy or flow cytometry (Campbell & Vaulot, 1993; Campbell et al., 1994; Li et al., 1983; Liu et al., 2007). While this approach may yield detailed information, it requires significant amounts of time and taxonomic expertise. As a result, data on the global spatial and temporal distributions of picophytoplankton are still sparse and the importance of picophytoplankton in marine biogeochemical processes is yet to be fully understood.

Remote sensing of picophytoplankton has been attempted by detecting the distributions of their optically active pigments such as chlorophyll *a* (Chl_*a*) and phycocyanin (Kuster et al., 2006; Randolph et al., 2008; Ruiz-Verdú et al., 2008). Chl_*a* is a common pigment existing in almost all phytoplankton (Jeffrey et al., 1997). Its concentration is roughly associated with the structure of phytoplankton community such that high and low Chl_*a* concentrations indicate a large proportion of microphytoplankton and picophytoplankton respectively in the phytoplankton community (Chisholm, 1992; Hirata et al., 2011; Pan et al., 2010, 2011; Uitz et al., 2006). However, partitioning and transposing Chl_*a* into the distribution of picophytoplankton species, as well as other phytoplankton, is still a challenge although chemotaxonomic methods have been recently attempted (Aiken et al., 2008; Alvain et al., 2005; Hirata et al., 2011; Pan et al., 2010, 2011). Phycocyanin is an important accessory

* Corresponding author. Tel.: +886 2 26539885x861; fax: +886 2 27833584.
E-mail addresses: xpan@gate.sinica.edu.tw, xpanx001@gmail.com (X. Pan).

0034-4257/$ – see front matter © 2012 Elsevier Inc. All rights reserved.
http://dx.doi.org/10.1016/j.rse.2012.10.014

pigment of a principal species of picophytoplankton, cyanobacteria (Jeffrey et al., 1997). Many studies have shown that its distribution may be related to cyanobacterial blooms, especially in the turbid inland lakes and the coastal waters (Kuster et al., 2006; Randolph et al., 2008; Ruiz-Verdú et al., 2008). There are at least three limitations in inferring the distribution of picophytoplankton using phycocyanin estimated through satellite remote sensing. First, phycocyanin is not a ubiquitous pigment found in all species of picophytoplankton. It is absent in prochlorophytes (Jeffrey et al., 1997) which contribute significantly to picophytoplankton biomass in the oligotrophic waters (Campbell & Vaulot, 1993; Campbell et al., 1994; Li et al., 1983; Liu et al., 2007). Total picophytoplankton biomass, thus, cannot be deduced easily from the concentration of phycocyanin alone. Secondly, phycocyanin is not a pigment that is unique to cyanobacteria. It may also be found in nano- and micro-phytoplankton such as diatoms and cryptophytes (Jeffrey et al., 1997). Therefore, the biomass of cyanobacteria cannot be accurately represented by the concentration of phycocyanin alone. Diatoms and cryptophytes are not expected to contribute significantly to total phytoplankton biomass in the oligotrophic waters, but they can become dominant in mesotrophic waters (Hirata et al., 2011; Pan et al., 2010, 2011). Thirdly, the absorption maximum of phycocyanin is located at around 630 nm (Kuster et al., 2006; Randolph et al., 2008; Ruiz-Verdú et al., 2008). This wavelength is not a nominal band in the widely used satellite sensors such as the Sea-viewing Wide Field-of-view Sensor (SeaWiFS) and the MODerate-resolution Imaging Spectrometers at Aqua sensor (MODIS-Aqua) and at Terra sensor (MODIS-Terra). Thus, the concentration of phycocyanin cannot be estimated from the data provided by these sensors with a high degree of sensitivity and accuracy.

Based on direct *in situ* observations, Alvain et al. (2005) reported that water with different phytoplankton community structure may be distinguished from each other by the ratios of the accessory pigments to Chl_*a*. Zeaxanthin (Zea) and fucoxanthin (Fuco) are especially useful as the former is found primarily in cyanobacteria and prochlorophytes, while the latter is a major accessory pigment in diatoms (Jeffrey et al., 1997), and these three phytoplankton, in addition to haptophytes, constitute the principal phytoplankton groups in the oceans (Alvain et al., 2005). Thus, a high ratio of Zea/Chl_*a* suggests that picophytoplankton may be dominant in the water while a high ratio of Fuco/Chl_*a* may indicate that the nano- and micro-phytoplankton, the diatoms, are dominant. Independently, Pan et al. (2010) reported an approach for deducing the concentrations of major phytoplankton pigments, including Chl_*a*, Zea and Fuco, in the coastal waters of the northeastern United States from remotely sensed data obtained from the SeaWiFS and MODIS-Aqua sensors. Therefore, combining these two approaches may provide a tool for evaluating the relative dominance of the picophytoplankton and the nano- and micro-phytoplankton from remotely sensed data. Here, we report the first attempt to estimate simultaneously the phytoplankton composition and the cell abundances of three picophytoplankton categories, *Prochlorococcus*, *Synechococcus*, and pico-eukaryotes, in the oceans from remote sensing data by using this combined approach and applying it to the northern South China Sea (NSCS).

2. Data and methods

2.1. Study area

The South China Sea (SCS) is the largest marginal sea in the tropical and temperate zones. It is a semi-enclosed basin extending from 23° N to 3° S and from 102° E to 121° E in the tropical and subtropical western Pacific Ocean with a maximum depth of over 5000 m. The South China Sea is connected to the East China Sea, the Java Sea, and the Sulu Sea to the north, south, and east respectively, through shallow straits. At its northeast corner, it is connected to the western Philippine Sea through the deep Luzon Strait where exchanges of intermediate and deep waters may occur (Shaw, 1989; Shaw & Chao, 1994). The northern half of the SCS, the northern SCS (NSCS), lies mostly in the subtropics. It is rimmed by a broad and extensive shelf system, the northern South China Sea Shelf-sea (NSCS Shelf-sea), along its northwestern border at the coasts of southern China and Vietnam. The Luzon Strait and the Luzon Island form its eastern boundary.

The waters in the central basin of the NSCS are warm and oligotrophic. The sea surface temperature typically varies between 20 and 30 °C, and the surface Chl_*a* varies from below 0.1 mg m^3 in the summer to exceeding 0.3 mg m^3 in the winter (Tseng et al., 2005). The dominant phytoplankton species are typically picophytoplankton, such as *Prochlorococcus* and *Synechococcus* (Agawin et al., 2003; Liu et al., 2007; Shiozaki et al., 2010; Wu et al., 2003). Towards the coast, and especially in the river plume area, phytoplankton biomass can be more than an order of magnitude higher (this study). Microphytoplankton and nanophytoplankton become more abundant and even dominant over picophytoplankton (Chen et al., 2007; Qiu et al., 2010).

Distinct monsoonal seasons are found in the NSCS: the stronger northeast monsoon between October and April and the weaker southwest monsoon between June and September. The combination of surface cooling and the stronger wind enhances vertical mixing and elevates biological production in the winter (Chen et al., 2006; Tseng et al., 2005). This results in a distinct seasonal pattern in biological productivity that is unique among tropical and subtropical waters. Because of the seasonally alternating wind direction and the orientations of the coast lines, wind driven coastal upwelling and the associated high biological productivity can be found at multiple locations in the NSCS. Upwelling has been reported along the east coast of Vietnam in the summer and northwest of the Luzon Island in the winter (Shaw et al., 1996; Tang et al., 2006). Topographically induced upwelling has also been found to occur at the Taiwan Bank and along the coasts of southern China in the NSCS Shelf-sea (Hong et al., 2009; Tang et al., 2002). A major river, the Pearl River (Zhujiang), drains into the NSCS from the northwest. Its peak flow occurs in the summer. This input of terrestrial material exerts a significant influence on the physics, biology and biogeochemistry in the inner and even the middle shelf of the NSCS Shelf-sea (Chen & Chen, 2006; Dai et al., 2008; Gan et al., 2010).

The NSCS is also a region that is subject to significant and persistent impacts of internal waves. These waves are generated at the Luzon Strait (Liu et al., 2006; Zhang et al., 2011; Zhao et al., 2004). Some propagate westward into the NSCS and eventually undergo transformation and dissipation in the shallower waters on the continental slope and shelf (Liu et al., 2006; Zhang et al., 2011; Zhao et al., 2004). These internal waves promote vertical exchange and bring nutrients from the subsurface waters to the mixed layer to fuel biological production (Pan et al., 2012; Wang et al., 2007). Other episodic and regional events that can affect biological productivity have also been reported to occur in the NSCS. They include meso-scale eddies (Lin et al., 2010), tropical cyclones (Lin et al., 2003), and atmospheric deposition (Lin et al., 2011). The former two processes can also enhance vertical mixing and elevate biological productivity. Nutrients from atmospheric deposition may stimulate photosynthetic activity directly while atmospherically derived iron may also promote primary production through nitrogen fixation (Lin et al., 2011; Mills et al., 2004). However, the effects of these episodic events last from days to weeks and do not extend beyond a limited geographical area (Lin et al., 2003, 2010, 2011).

2.2. Field experiments

Three cruises, covering the inner shelf to the deep central basin of the NSCS, were conducted between 2008 and 2010 (Fig. 1 and Table 1). In addition to standard hydrographic stations, anchored stations for time-series observations of up to 36 h long were occupied in the inner shelf in the Pearl River plume and at the continental slope over the Dongsha Atoll (Fig. 1). The SouthEast Asian Time-series Study (SEATS) station was occupied 6 times for up to 44 h between September 2002 and July 2005 (Fig. 1 and Table 1).

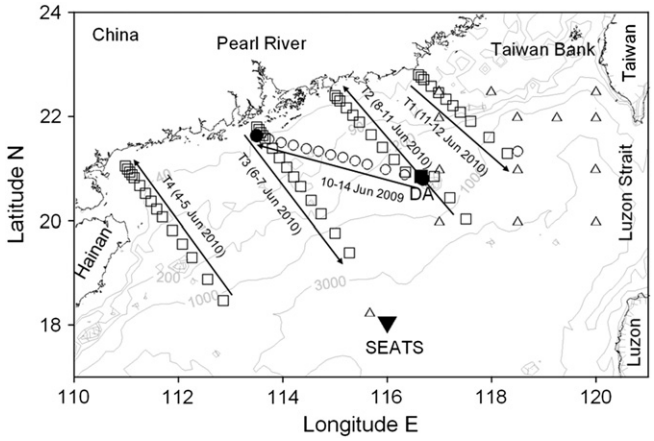

Fig. 1. Station locations in the northern South China Sea (NSCS). Δ – Cruise OR1_866 (28 May to 6 June 2008); ○ – OR3_1379 (10 to 14 June 2009); □ – OR1_929 (4 to 13 June 2010); ●, ■ – Time-series anchored stations during OR3_1379 and OR1_929, respectively; ▼ – the SouthEast Asian Time-series Study (SEATS) station; DA – the Dongsha Atoll. →: sampling sequence and sampling periods in June 2009 and 2010.

At each hydrographic station, the depth-distributions of temperature and salinity were recorded with a conductivity–temperature–depth (CTD) recorder (SeaBird SBE9/11). Discrete water samples were collected with depth by using Go-Flo bottles mounted onto a Rosette sampling assembly (General Oceanic) for the determination of phytoplankton pigments and cell counts. At the anchored stations and at the SEATS station, additional CTD profiles and discrete water samples were obtained in time intervals of 1 to 3 h.

Phytoplankton cells were collected with GF/F filters and then frozen immediately in liquid nitrogen. These samples were stored frozen at −80 °C until they were analyzed by high-performance liquid chromatography (HPLC) (Bidigare et al., 2002). The selected HPLC pigments applied in this study include: total chlorophyll *a* (TChl_*a*; the sum of monovinyl Chl_*a*, divinyl Chl_*a*, and chlorodide *a*), fucoxanthin (Fuco), zeaxanthin (Zea) and 19′-hexanoyloxyfucoxanthin (Hex). Cell counting samples were preserved with paraformaldehyde and stored in the liquid nitrogen until they were analyzed for the abundances of three picophytoplankton categories, *Prochlococcus*, *Synechococcus* and pico-eukaryotes, by flow cytometry (Liu et al., 2007; and references therein). Individual species of photosynthetic pico-eukaryotes cannot yet be quantified by flow cytometry alone. The dominant phytoplankton groups in the pico-eukaryotes are likely the haptophytes and the chlorophytes. However, they can be found in most algal classes (Vaulot et al., 2008).

2.3. NOMAD ocean color data set

A compilation of the worldwide *in situ* measurements of phytoplankton HPLC pigments, water-leaving radiance (L_w), water surface downwelling irradiance (E_s), and optimally integrated sea surface temperature (SST) were obtained from the NASA bio-Optical Marine Algorithm Data (NOMAD, v2.a) (Werdell & Bailey, 2005). Remote sensing reflectance (R_{rs}) was calculated as: $R_{rs}(\lambda)=L_w(\lambda)/E_s(\lambda)$ (Mobley, 1994). The bands (λ) at 443, 465, 489, 530 and 555 nm were used to estimate the phytoplankton pigments according to spectral characteristics of pigments and previous works (Bricaud et al., 2004; Pan et al., 2008, 2010). For each of the selected bands, if a direct measurement was not available, $R_{rs}(\lambda)$ was estimated from a linear integration by using R_{rs} at two closest bands available in the NOMAD. As only R_{rs} at 443, 469, 488, 531, and 555 nm were available by MODIS, R_{rs} at 465, 489 and 530 nm were not available. Thus, R_{rs} at 489 and 530 nm were assumed to be equivalent to R_{rs} at 488 and 531 nm. $R_{rs}(465)$ was estimated from $R_{rs}(443)$ and $R_{rs}(488)$ (Fig. S1 in the auxiliary material) so that our approach was readily applicable to other satellite sensors, such as the SeaWiFS.

$$R_{rs}(465) = 0.5405R_{rs}(443) + 0.4727R_{rs}(488) \quad (1)$$

Thus, the R_{rs} at all the five wavelengths needed could be estimated from the MODIS data source. Overall, there were 1275 observations with match-up measurements of HPLC pigments and $R_{rs}(\lambda)$. Algorithms for estimating the concentrations of TChl_*a*, Fuco, and Zea from R_{rs} band ratios were derived empirically according to the methods of Pan et al. (2008, 2010).

2.4. Satellite imagery

MODIS-Aqua Level-2 products, including R_{rs} and nighttime (4 μm) sea surface temperatures (SST), between 17 and 24° N, and 110 and 121° E were downloaded from the NASA Ocean Color Web (http://oceancolor.gsfc.nasa.gov/). The selected nominal R_{rs} bands included 443, 488, 531, 555, 645, 667, and 678 nm. $R_{rs}(465)$ was estimated from $R_{rs}(443)$ and $R_{rs}(488)$ by using Eq. (1). The MODIS-Aqua images are in Merged Local Area Coverage (MLAC) with a native resolution of ~1 km. Satellite images were mapped isotropically to 111 pixels per degree of longitude or latitude (at an approximate resolution of 1 km × 1 km per pixel) through the SeaWiFS Data Analysis System software (SeaDAS; version 6.2). The concentrations of phytoplankton pigments and the abundances of picophytoplankton for the MODIS-Aqua data were estimated from the empirical algorithms developed in this study.

The satellite-derived products were validated by comparing them to *in situ* observations, following the protocols of Bailey and Werdell (2006). The satellite overpass time window was expanded to ±48 h of the field observations. Ideally, a narrower window, ±3 h, is preferred (Bailey & Werdell, 2006). A wider window was used here because of the paucity of remotely sensed data from the study area as a result of the frequent cloud cover. At a window of ±3 h, there was almost no match-up data between the satellite observations and the field measurements. The wider window used likely has introduced additional uncertainty into the comparison as a result of the temporal effect (Pan et al., 2008, 2010). Thus, the comparison in this study likely represents a worst case scenario.

The goodness of fit between the derived products and the field observations is assessed by the mean absolute percentage difference (MAPD) and the root mean square error (RMSE) such that:

$$MAPD = \sum \frac{|P_{derived} - P_{field}|}{nP_{field}} \times 100\% \quad (2)$$

$$RMSE = \sqrt{\sum [\log(P_{derived}) - \log(P_{field})]^2 / n} \quad (3)$$

Here, n represents the number of samples, while $P_{derived}$ refers to each of the derived products and P_{field} is the corresponding field measurement. The RMSE is based on a log-scale unless noted.

Table 1
Field experiments conducted and the selected parameters used for this study.

Cruises	Periods	Parameters[a]	Stations[b]
OR1_866	28 May to 6 Jun 2008	CTD, HPLC	14 (14)
OR3_1379	10 to 14 Jun 2009	CTD, HPLC, CC	14 (14)
OR1_929	4 to 13 Jun 2010	CTD, Nut, HPLC, CC	54 (29)
SEATS	4 Sep 2002; 8 to 9 Nov 2004; 22 Jan, 30 Mar, 30 Jul 2005	CTD, Fluo, CC	6 (6)

[a] CTD – the conductivity-temperature-depth records; HPLC – phytoplankton pigments by high-performance liquid chromatography; CC – cell counting by flow cytometry; Nut – nutrients; Fluo – chlorophyll *a* concentration determined by fluorometry.
[b] Number of stations in which water samples were collected is shown in parenthesis.

3. Results and discussions

3.1. Surface hydrographic and phytoplankton characteristics: field in situ observations

Both the hydrographic conditions and the distribution of phytoplankton in the NSCS Shelf-sea are known to be highly variable spatially and seasonally (Chen et al., 2007; Qiu et al., 2010; Shaw & Chao, 1994; Tseng et al., 2005; Wong et al., 2007). An example of the cross-shelf variations in the hydrological and biological characteristics along a transect from the Pearl River mouth to the central basin (transect T3 in Fig. 1) in June 2010 is shown in Fig. 2. This transect can be sub-divided roughly into four sections: the inner shelf (water depth $z \leq 40$ m), the middle shelf ($40 < z \leq 90$ m), the outer shelf ($90 < z \leq 200$ m), and the open NSCS ($z > 200$ m). In the inner shelf, the water column was relatively well mixed, and the oceanographic conditions might be heavily influenced by coastal processes. In the outer shelf and the open NSCS, the influence of oceanic processes became dominant. The middle shelf was a transition zone between the inner shelf and the outer shelf. Surface water temperatures were around 26.5, 27 and 27 to 28 in the inner, middle and outer shelf, and approaching 29 °C in the open NSCS (Fig. 2a). Surface salinity stayed within a narrow range between 33.3 and 34.0 beyond the river plume, but it dropped to 31.0 at the most coastward station (Fig. 2a). The mixed-layer depth (MLD), which is defined as the depth at which the temperature is 0.5 °C lower than the surface temperature, across the transect generally varied between a narrow range of 25 to 35 m (Fig. 2b), consistent with previous studies in the summer (Liu et al., 2002; Tseng et al., 2005). However, it fluctuated conspicuously at the outer shelf, reaching depths around 50 m (Fig. 2b). This might have resulted from the effect of internal waves which have been reported to occur commonly in this zone (Liu et al., 2006; Pan et al., 2012; Zhang et al., 2011; Zhao et al., 2004).

The concentrations of TChl_*a*, Zea, and Fuco in the surface waters in June generally decreased seaward from 0.4, 0.1 and 0.04 mg m^{-3} respectively in the inner shelf to 0.1, 0.07 and <0.005 mg m^{-3} in the outer shelf and 0.1, 0.02 and <0.001 mg m^{-3} in the open NSCS (Fig. 2c). In terms of cell counts, *Prochlorococcus* were generally the most abundant picophytoplankton except in the inner shelf (Fig. 2d). In the open NSCS, they were typically one-order and two-orders of magnitude higher than *Synechococcus* and pico-eukaryotes respectively (Fig. 2d), as had been reported previously (Liu et al., 2007). The proportion of *Prochlorococcus* in the picophytoplankton community tended to decrease shoreward. In the inner shelf, *Synechococcus* might become more abundant than *Prochlorococcus*.

The transect shown in Fig. 2 was sampled on 6 to 7 June 2010, as a part of a summer cruise between 4 and 13 June 2010 (Table 1 and Fig. 1), during which the discharge of the Pearl River (~1.0×10^4 m^3 s^{-1}) was only about 70% of the climatological average in the month of June (1.4×10^4 m^3 s^{-1}) (Fig. 3). The peak discharge (~2.4×10^4 m^3 s^{-1}) did not arrive until 16 June 2010 after the cruise (Fig. 3). As a result, the river plume was less influential, surface salinity was quite uniform across the transect, and significantly fresher water was found only at the most coastward station which was located at about 30 km from the coast (Fig. 2). More pronounced depression in salinity and elevation in TChl_*a* had been observed in the Pearl River estuary in June in other years (Yin, 2002). In June 2009, the peak discharge of the Pearl River (~2.0×10^4 m^3 s^{-1}) was about 40% higher than the climatological mean in the month of June (Fig. 3). Correspondingly, our data indicated a prominent drop in salinity to a minimum of 8.9 and an increase in TChl_*a* to 16 mg m^{-3} in the surface water in the inner shelf.

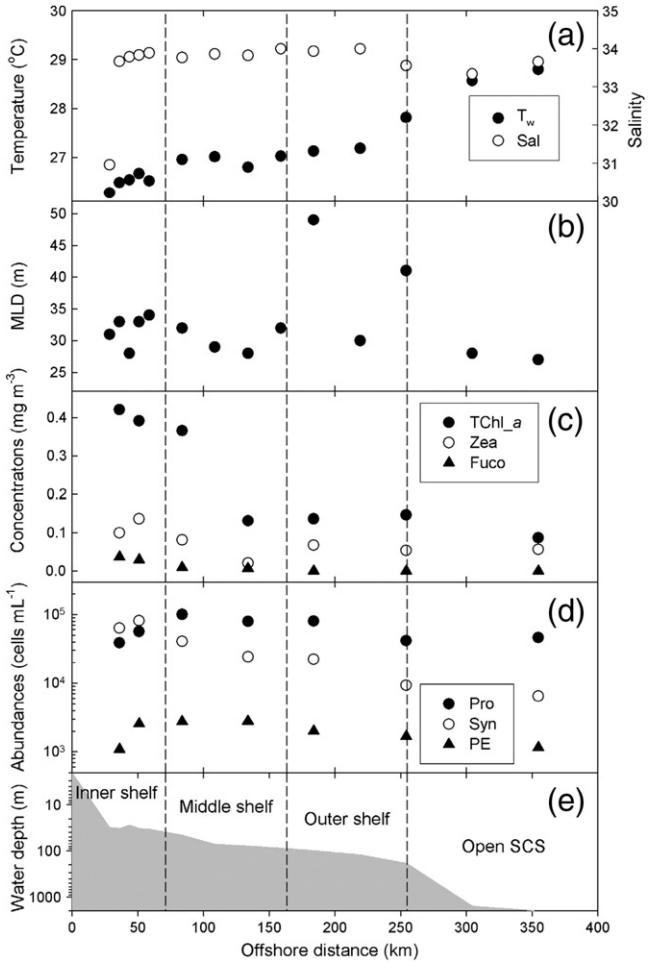

Fig. 2. Variations in (a) water temperature (T_w) and salinity (Sal); (b) mixed-layer depth (MLD); (c) concentrations of total chlorophyll *a* (TChl_*a*), zeaxanthin (Zea), and fucoxanthin (Fuco); (d) cell abundances of *Prochlorococcus* (Pro), *Synechococcus* (Syn), and pico-eukaryotes (PE); and (e) water depth along transect T3 in June 2010. ---: dividing line between hydrographic sub-regions.

3.2. Classification of water by dominant phytoplankton group

Based on direct measurements on their pigment composition and the spectral characteristics of these pigments, Alvain et al. (2005) proposed a scheme for identifying the four major phytoplankton groups in the global ocean, namely, *Prochlorococcus*, *Synechococcus*-like cyanobacteria, haptophytes and diatoms, by using a set of threshold values in the ratios of four accessory pigments, namely, divinyl chlorophyll *a* (DV_*a*), fucoxanthin (Fuco), 19′-hexanoyloxyfucoxanthin (Hex), and zeaxanthin (Zea), to TChl_*a* (Table 2) and classifying

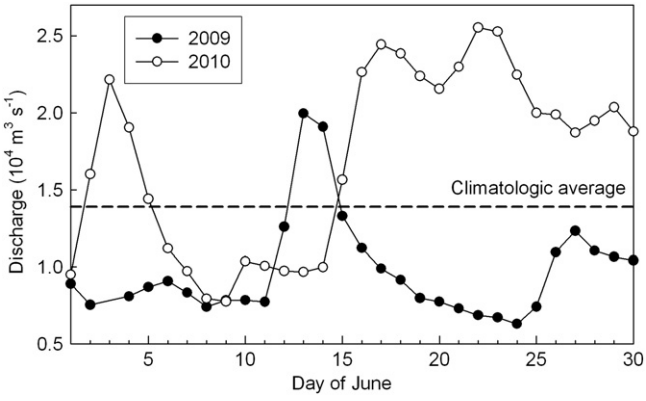

Fig. 3. Daily discharge of the Pearl River in June 2009 and June 2010 at the Wuzhou Station on the West River, a major tributary accounting for ~70% of the Pearl River discharge (the Bureau of Hydrology Information Center of Water Resources, China; http://xxfb.hydroinfo.gov.cn/EN/eindex.jsp). ---: climatological (2005 to 2010) average discharge in June.

Table 2
The major phytoplankton groups and the corresponding criteria of the ratios of accessory pigments to TChl_*a*.

Dominant species	TChl_*a*	Ratios of accessory pigments to TChl_*a*			
		DV_*a*	Fuco	Hex	Zea
(a) Criteria used by Alvain et al. (2005)					
Prochlorococcus	–	>0.40	–	–	>0.35
Synechococcus	–	<0.40	–	–	>0.20
Haptophytes	–	<0.40	–	>0.14	<0.20
Diatoms	–	<0.40	>0.18	–	<0.20
(b) Criteria used in this study					
Prochlorococcus	<0.3	–		–	≥0.35
Synechococcus	≥0.3	–	–	–	≥0.35
	–	–	–	–	0.20–0.35
Haptophytes	–	–	<0.18	–	<0.20
Diatoms	–	–	≥0.18	–	<0.20

the waters in the oceans according to the dominant phytoplankton groups. Although six accessory pigments (the above four plus peridinin and pheophytin *a*) were mentioned in Alvain et al. (2005), only the above four were needed to distinguish among the four principle phytoplankton groups. However, in view of the difficulties in estimating the concentrations of DV_*a* and Hex from remotely sensed data (Pan et al., 2010), their scheme was modified and simplified here so that these major phytoplankton groups might be identified by using only two accessory pigments (Fuco and Zea) in addition to TChl_*a* (Table 2). In this modified scheme, first, by following the scheme of Alvain et al. (2005), the phytoplankton groups of *Prochlorococcus* and *Synechococcus* were distinguished from the phytoplankton groups of haptophytes and diatoms by their enrichment in Zea using the threshold value of Zea/TChl_*a*>0.20. Then, also as in Alvain et al. (2005), a component of *Synechococcus* could be distinguished from *Prochlorococcus* by its lower Zea/TChl_*a* (0.20 to 0.35) relative to that (>0.35) of *Prochlorococcus*. Based on Zea/TChl_*a* alone, the remaining component of *Synechococcus* was indistinguishable from *Prochlorococcus* since both would have values of Zea/TChl_*a*>0.35. Alvain et al. (2005) used the higher DV_*a*/TChl_*a* (>0.4) in *Prochlorococcus* in comparison to *Synechococcus* for distinguishing these two groups of picophytoplankton from each other (Table 2). However, on a further examination of the NOMAD data, it was apparent that the high ratio of DV_*a*/TChl_*a* (>0.2) was invariably associated with low TChl_*a* (<0.3 mg m^{-3}) (Fig. 4a). Thus, *Synechococcus* could be distinguished from *Prochlorococcus* by: (a) 0.2<Zea/TChl_*a*<0.35 irrespective of the concentration of TChl_*a*; and (b) TChl_*a*≥0.3 when Zea/TChl_*a* exceeded 0.35 (Table 2).

Alvain et al. (2005) used two separated criteria in two pigments for distinguishing diatoms from haptophytes such that Fuco/TChl_*a*>0.18

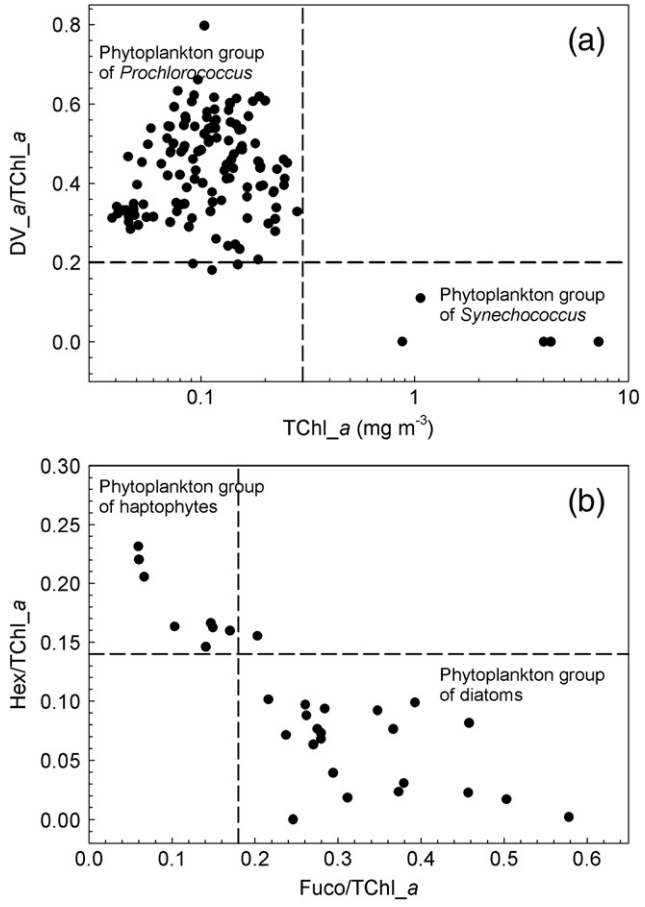

Fig. 4. Relationship between (a) DV_*a*/TChl_*a* and TChl_*a* at Zea/TChl_*a*>0.35; and (b) Hex/TChl_*a* and Fuco/TChl_*a* in diatoms or haptophytes dominated NSCS surface waters. --- in (a): TChl_*a*=0.3 mg m^{-3} or DV_*a*/TChl_*a*=0.2; --- in (b): Fuco/TChl_*a*=0.18 or Hex/TChl_*a*=0.14.

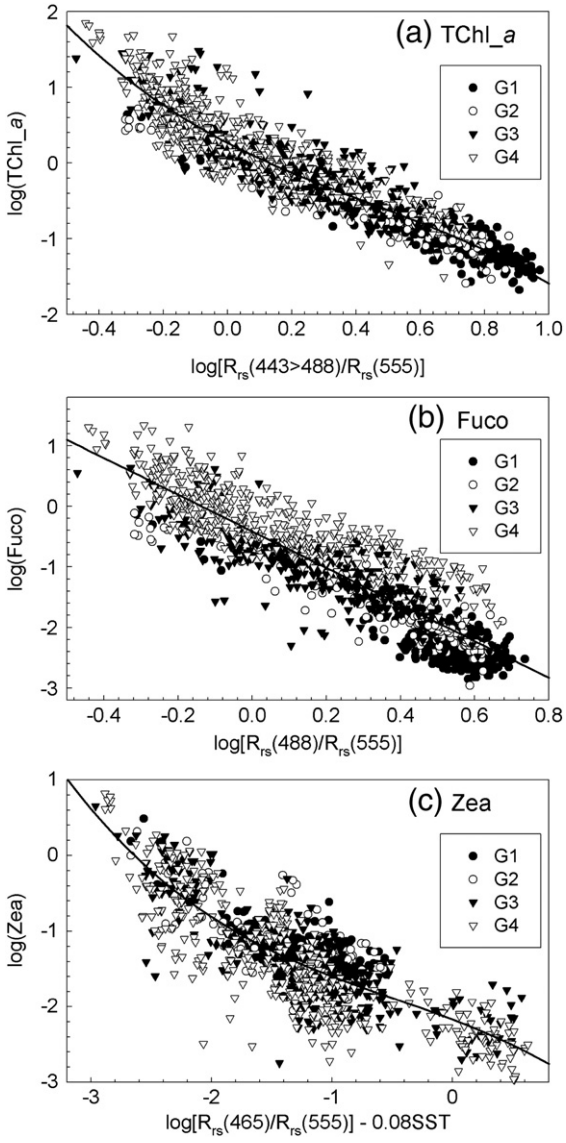

Fig. 5. Non-phytoplankton group specific relationship between (a) TChl_*a*, (b) Fuco, and (c) Zea and radiometric measurements and/or sea surface temperature (SST). —: best fit line; G1, G2, G3, G4: samples dominated by *Prochlorococcus*, *Synechococcus*, haptophytes, and diatoms, respectively.

Table 3
The derived coefficients of Eq. (4) in relating the pigment concentrations to remote sensing reflectance (R_{rs}) and sea surface temperature (SST) under various phytoplankton groups.

Pigments	Groups	[a] X	n	B_0	B_1	B_2	B_3	r^2	RMSE	MAPD (%)
(a) Non-phytoplankton group specific algorithms										
TChl_*a*	All	$\log[R_{rs}(443>488)/R_{rs}(555)]$	1275	0.2640	−2.195	1.323	−0.9869	0.874	0.253	47.9
	All	$\log[R_{rs}(443>488)/R_{rs}(531)]$	1137	0.2386	−3.223	1.979	−1.142	0.850	0.277	52.6
Fuco	All	$\log[R_{rs}(488)/R_{rs}(555)]$	1220	−0.4135	−3.022	–	–	0.816	0.417	87.9
	All	$\log[R_{rs}(488)/R_{rs}(531)]$	1082	−0.4756	−4.458	–	–	0.783	0.440	93.2
Zea	All	$\log[R_{rs}(465)/R_{rs}(555)]-0.08SST$	1241	−2.169	−0.6046	−0.1065	−0.0745	0.684	0.348	76.8
	All	$\log[R_{rs}(465)/R_{rs}(531)]-0.05SST$	1103	−2.166	−0.9122	−0.1502	−0.2191	0.682	0.364	82.8
(b) Phytoplankton group specific algorithms										
Fuco	Prokaryotes	$\log[R_{rs}(488)/R_{rs}(555)]$	418	−0.9116	−2.471	–	–	0.818	0.248	39.5
	Haptophytes	$\log[R_{rs}(488)/R_{rs}(555)]$	344	−0.7076	−2.129	1.728	−3.273	0.681	0.327	65.4
	Diatoms	$\log[R_{rs}(488)/R_{rs}(555)]$	458	−0.2521	−2.178	1.973	−2.589	0.743	0.320	69.2
	Prokaryotes	$\log[R_{rs}(488)/R_{rs}(531)]$	323	−0.9834	−3.631	–	–	0.826	0.259	40.9
	Haptophytes	$\log[R_{rs}(488)/R_{rs}(531)]$	311	−0.7322	−3.237	2.123	−7.324	0.653	0.349	68.4
	Diatoms	$\log[R_{rs}(488)/R_{rs}(531)]$	448	−0.2562	−3.328	2.324	−3.125	0.701	0.343	75.0
Zea	Prokaryotes	$\log[R_{rs}(465)/R_{rs}(555)]-0.02SST$	465	−1.129	−0.9014	−0.6966	−1.340	0.763	0.181	35.8
	Eukaryotes	$\log[R_{rs}(465)/R_{rs}(555)]-0.05SST$	776	−2.141	−0.6859	0.1438	−0.0924	0.730	0.372	84.9
	Prokaryotes	$\log[R_{rs}(465)/R_{rs}(531)]-0.01SST$	370	−1.057	−1.335	0.0927	−1.820	0.756	0.199	40.7
	Eukaryotes	$\log[R_{rs}(465)/R_{rs}(531)]-0.04SST$	733	−2.237	−0.8018	0.5273	−0.0215	0.728	0.380	88.4

[a] $R_{rs}(443>488)=\max[R_{rs}(443), R_{rs}(488)]$ for MODIS.

indicated the dominance of diatoms while Hex/TChl_*a*>0.14 indicated the dominance of haptophytes. In our field *in situ* observations where all three pigments were measured, Hex/TChl_*a* exceeding 0.14 was found when Fuco/TChl_*a* dropped below 0.18 (Fig. 4b). Thus, the dominance of haptophytes, in which Fuco/TChl_*a*<0.18, could be distinguished from the dominance of diatoms, in which Fuco/TChl_*a*≥0.18, by their Fuco content alone (Table 2).

3.3. Development of algorithms

3.3.1. Non-phytoplankton group specific algorithms for estimating pigment concentrations

The relationships between the concentrations of the pigments and the remotely sensed measurements are shown in Fig. 5. The pigment concentrations could be expressed as third-order polynomial functions of the radiometric observations such that:

$$Y = B_0 + B_1X + B_2X^2 + B_3X^3 \quad (4)$$

Here, Y represents log(TChl_*a*), log(Fuco), or log(Zea), X is an expression of R_{rs} band ratio without (for TChl_*a* and Fuco) or with (for Zea) the embedding of sea surface temperature (SST), and B_0, B_1, B_2, and B_3 are the derived coefficients. The results are shown in Table 3 and Fig. 5. Two sets of algorithms, based on the R_{rs} ratios to $R_{rs}(555)$ and $R_{rs}(531)$, were developed (Table 3). The former set yielded relationships with lower RMSEs and MAPDs but $R_{rs}(555)$ was more prone to errors in the correction for atmospheric effect in oligotrophic waters. The extent of this effect could be assessed from the corresponding $R_{rs}(645)$, $R_{rs}(667)$ and $R_{rs}(678)$. If these values were negative, they suggested an over-correction in the atmospheric effect and the algorithms based on the ratios to $R_{rs}(531)$ were used.

The RMSEs of the relationships were about 0.26, 0.35 and 0.43 for TChl_*a*, Zea and Fuco, respectively (Table 3). The corresponding MAPDs ranged between 50% and 90% (Table 3). The errors in the relationships for Zea and Fuco were relatively large. A closer examination of these relationships indicated that they might be phytoplankton group specific as the data points of each phytoplankton group tended to skew towards a different trend relative to the best fit line (Fig. 5). Thus, phytoplankton group specific algorithms should improve the relationships. On the other hand, the relationship for TChl_*a* was not phytoplankton group specific as the data points from each group were distributed randomly over the best fit line (Fig. 5).

3.3.2. Phytoplankton group specific algorithms for estimating pigment concentrations

The NOMAD data set was sub-divided into the four principal phytoplankton groups by applying our modified classification of Alvain et al. (2005) as described in Section 3.2 to their pigment compositions. Then, the relationship between the concentrations of the two accessory pigments and the remotely sensed measurements in each sub-data set was again fitted to a third order polynomial function as described in Section 3.3.1. The relationships for the groups of *Prochlorococcus* and *Synechococcus* were indistinguishable from each other. These data were pooled together and a single relationship for these two groups of prokaryotes was derived. For the haptophytes and diatoms, their relationships to Zea were similar to each other. These data were again pooled and a single relationship for these two groups of eukaryotes was derived. The results are tabulated in Table 3 and shown in Fig. 6. Relative to the non-phytoplankton group specific relationships, in most cases, both RMSEs and MAPDs of the phytoplankton group specific relationships were significantly smaller, being reduced by about 40% to 50%. There was no improvement in the relationship to Zea for the eukaryotes. The RMSEs and MAPDs were smaller when $R_{rs}(555)$ rather than $R_{rs}(531)$ was used in the relationships. By using these phytoplankton group specific relationships relative to $R_{rs}(555)$, the RMSE and MAPD could be reduced to below 0.25 and 40% for the groups of the prokaryotes and below 0.37 and 85% for the groups of the eukaryotes.

3.3.3. Algorithms for estimating species specific cell abundance

By using the direct *in situ* observations in the northern South China Sea, the cell abundances of *Prochlorococcus* (N_{Pro}), *Synechococcus* (N_{Syn}), and pico-eukaryotes (N_{PE}) could be empirically related to TChl_*a* and Zea in waters dominated by the prokaryotes, the haptophytes, or the diatoms such that:

$$\log(N) = A_0 + A_1Y_1 + A_2{Y_1}^2 + A_3Y_2 + A_4{Y_2}^2 \quad (5)$$

Here N represents N_{Pro}, N_{Syn}, or N_{PE}, $Y_1=\log(\text{TChl\_}a)$, and $Y_2=\log(\text{Zea})$. The least-square solutions of the derived coefficients, A_0, A_1, A_2, A_3, and A_4, were generated by using the right matrix division function in the MATLAB® software, matrix[1, Y_1, Y_1^2, Y_2, Y_2^2]\matrix[log(N)], for each phytoplankton group. The results are shown in Table 4 and Fig. 7. The relationships were dependent on the phytoplankton composition. As a result, separate algorithms had to be developed for water with different dominating phytoplankton group. As a corollary, these algorithms

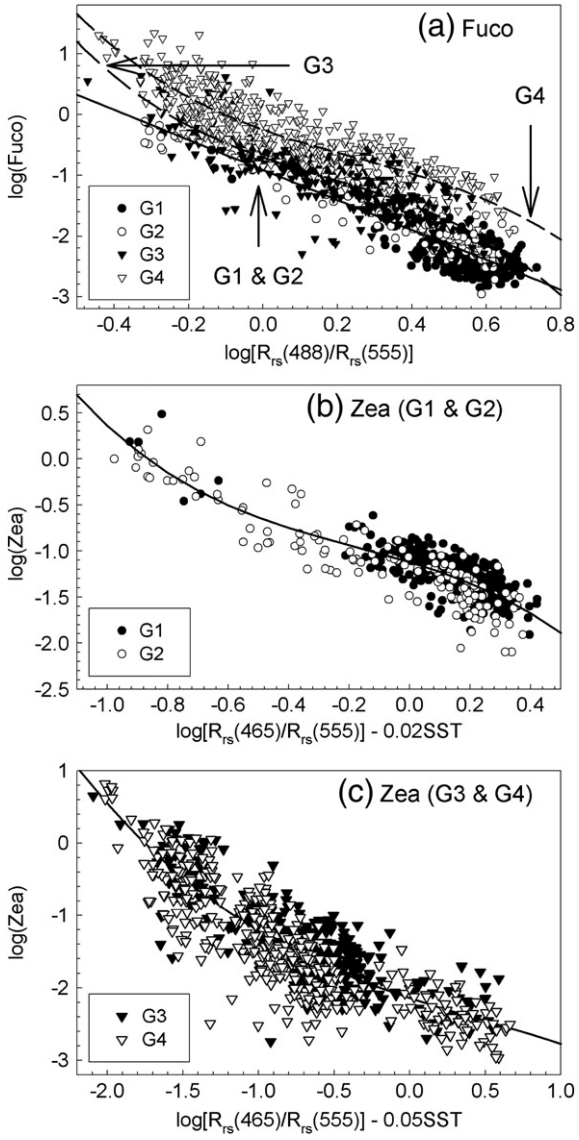

Fig. 6. Phytoplankton group specific relationships between (a) Fuco; (b) Zea in G1 and G2 samples; and (c) Zea in G3 and G4 samples and radiometric measurements and/or SST. - - - in (a): best fit lines for G3 or G4 samples; — in (a): best fit line for G1 and G2 samples; — in (b) and (c): best fit line for complete data set. G1, G2, G3, G4: as defined in Fig. 5.

could not be applied until the phytoplankton composition and the dominating phytoplankton group were determined. Pico-eukaryotes were not further fractionated into the individual phytoplankton classes because such data could not be obtained by flow cytometry. An examination of the algorithm performances in deriving the cell abundances in waters dominated by *Prochlorococcus* and *Synechococcus* individually indicated that they were similar to each other. Thus, the data were pooled and a single relationship was developed for waters dominated by either prokaryotes. The resulting RMSEs and MAPDs ranged between 0.13 and 0.37, and, 23% and 51%.

3.4. Data processing scheme for assessing the concentrations of pigments, phytoplankton composition and cell abundances from ocean color

Data processing was consisted of three principal parts (Fig. 8).

Part 1: A preliminary estimation of the concentrations of the pigments, TChl_*a*, Fuco and Zea, was made by applying the non-phytoplankton group specific algorithms developed in Section 3.3.1 to the remote sensing reflectance (R_{rs}) and sea surface temperature (SST) from MODIS-Aqua.

Part 2: A refined estimation of the concentrations of the three pigments and the associated phytoplankton group composition was made by iteration. The iterative procedure involved the following steps: (a) the phytoplankton composition was estimated from the pigment concentrations estimated in Part 1 by using the modified water classification described in Section 3.2; (b) the phytoplankton group specific algorithms developed in Section 3.3.2 were applied to the combination of the phytoplankton composition assessed in step (a) and the R_{rs} and SST from MODIS to provide an improved estimation of the concentrations of the pigments; (c) steps (a) and (b) were repeated by using the new estimates given in step (b). The iteration was terminated when the pigment concentrations and the phytoplankton composition converged towards constant values. In the few cases when no convergence could be reached, the results from the preliminary estimation in Part 1were used.

Part 3: The dominant phytoplankton group was identified from the phytoplankton composition given in Part 2. Then, the cell abundances of the three picophytoplankton categories, *Prochlorococcus*, *Synecococcus* and pico-eukaryotes, were estimated from the concentrations of TChl_*a* and Zea estimated in Part 2 by using the algorithms appropriate for the dominant phytoplankton group developed in Section 3.3.3.

3.5. Accuracy, uncertainties and validation

There were three primary sources of uncertainties in the estimations of phytoplankton pigments, phytoplankton composition, and cell abundances in the proposed protocol (Fig. 8): (a) the statistical uncertainties in relating the concentrations of the pigments from remotely sensed radiometric measurements (Eq. 4) and the cell abundances from the pigments (Eq. 5); (b) the correct assessment of the phytoplankton

Table 4
The derived coefficients of Eq. (5) in relating the pigment concentrations to the cell abundances of *Synechococcus* (N_{Syn}), *Prochlorococcus* (N_{Pro}), and pico-eukaryotes (N_{PE}) under various phytoplankton groups.

Dominant groups	Cell abundances	A_0	A_1	A_2	A_3	A_4	r^2	RMSE	MAPD (%)	Median $\log(N_{taxa})$
Prokaryotes (n = 301)	N_{Pro}	5.286	−0.563	−0.545	0.217	−0.136	0.552	0.205	40.1	4.854
	N_{Syn}	6.135	0.732	0.409	1.457	0.015	0.645	0.368	50.8	3.983
	N_{PE}	3.534	1.079	0.178	−0.731	−0.271	0.650	0.195	37.6	3.340
Haptophytes (n = 27)	N_{Pro}	5.350	−2.627	−1.350	0.256	−0.485	0.796	0.185	31.7	4.770
	N_{Syn}	4.119	1.906	0.947	−1.935	−0.965	0.712	0.290	40.1	4.529
	N_{PE}	2.255	2.080	1.128	−2.992	−1.062	0.836	0.127	23.3	3.824
Diatoms (n = 42)	N_{Pro}	5.539	0.327	−0.004	1.716	0.397	0.725	0.269	42.4	3.948
	N_{Syn}	5.635	−0.931	0.433	0.847	0.144	0.767	0.156	28.6	4.780
	N_{PE}	3.712	1.089	−0.319	−0.327	−0.224	0.491	0.255	37.0	3.935

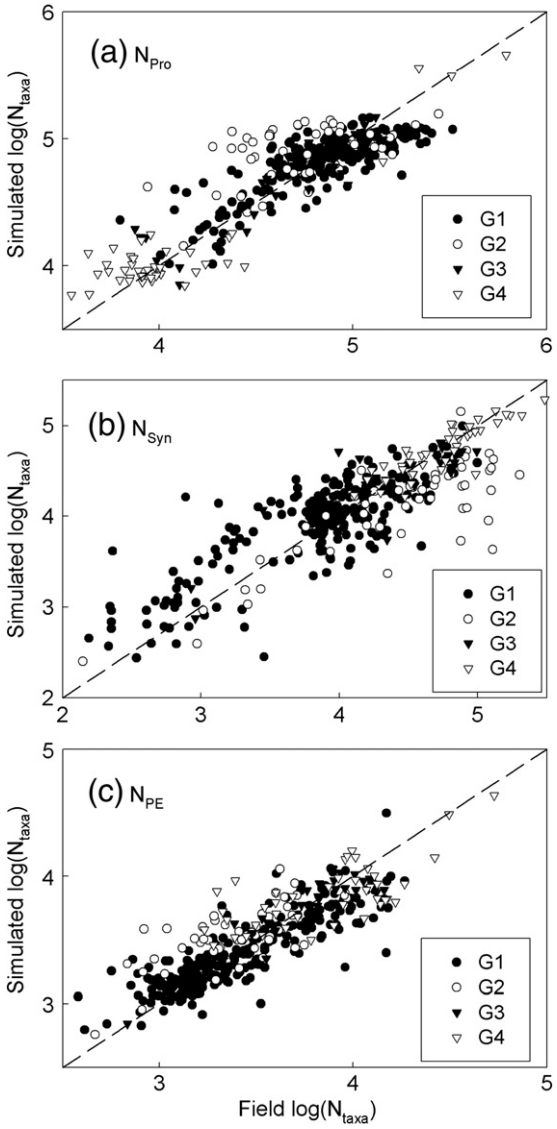

Fig. 7. Relationship between simulated and observed cell abundances of (a) *Prochlorococcus* (N_{Pro}), (b) *Synechococcus* (N_{Syn}), and (c) pico-eukaryotes (N_{PE}). G1, G2, G3, G4: as defined in Fig. 5; - - -, 1:1correspondence.

composition and the assignment of the dominant phytoplankton group by using the proposed modified classification; and (c) the propagation of the previous two sources of uncertainties to the estimation of the concentrations of the pigments and cell abundances from remotely sensed data. The first source of uncertainties was indicated in the RMSEs of the relationships in log-space, which fell within 0.2 to 0.4 for the concentrations of the pigments (Table 3) and 0.1 to 0.4 for the cell abundances (Table 4). These levels of uncertainties are considered generally acceptable in remote sensing research (IOCCG, 2006; O'Reilly et al., 1998; Pan et al., 2008, 2010). The effects of the other two sources of uncertainties were evaluated by comparing the results obtained from remote sensing to direct *in situ* observations. The match-up (within a time window of ±48 h) comparisons of the concentrations of TChl_*a*, Fuco, and Zea and the cell abundances of *Prochlorococcus*, *Synechococcus*, and pico-eukaryotes between those derived from the MODIS-Aqua observations and the field *in situ* measurements are shown in Fig. 9. The RMSEs in log-space in the comparisons were 0.17 to 0.39 for the pigments and 0.22 to 0.42 for the cell abundances while the corresponding MAPDs were around 31% to 43% and 29% to 55% respectively (Table 5). These results suggested that even allowing for the impact of short-term (hourly to diurnal) variations on the distributions of the pigments and the picophytoplankton abundances (Claustre et al., 2002) and temperature effect, the satellite-derived products from our approach agreed with the field measurements reasonably well. Because these comparisons were based on a time window of ±48 h, a better agreement might be expected in a synoptic match-up comparison (Pan et al., 2008, 2010). In addition to the above primary three, there might be some, possibly secondary, sources of uncertainty relevant to our approach. They may include: (a) applying a linear regression to estimate $R_{rs}(465)$ from $R_{rs}(443)$ and $R_{rs}(488)$ (Eq. 1), which might introduce an extra error in estimating Zea; (b) using Fuco (a biomarker pigment to diatoms) instead of Hex (a biomarker pigment to haptophytes) to determine the dominance of haptophytes (Table 2); and (c) the errors in the HPLC *in situ* measurements (Claustre et al., 2004) and in the flow cytometry cell count data (Pan et al., 2010).

3.6. Distributional patterns of phytoplankton pigments, phytoplankton composition and cell abundances in the NSCS

3.6.1. Spatial distributions in contrasting seasons in the NCSC

By using the approach developed in Sections 3.3 and 3.4, the phytoplankton pigments, phytoplankton composition and cell abundances in the NSCS in June and December 2009 were estimated and the results together with the distribution of sea surface temperature (SST) are shown in Fig. 10. In June, waters exceeding ~27 °C covered most of the NSCS. Cooler water, which originated from the terrestrial sources and the coastal current from the Taiwan Strait and further north (Gan et al., 2009a,b; Hu et al., 2010), with temperatures below ~26 °C was found only as a narrow strip in the northern portion of the inner shelf of the NSCS Shelf-sea. In contrast, in December, waters with temperatures below 26 °C covered almost the entire NSCS, and thus the entire NSCS Shelf-sea, north of about 18° N. The concentrations of the pigments in the open NSCS were typically low, with TChl_*a*, Fuco and Zea of around 0.1, 0.01 and 0.05 mg m^{-3} in June, and, around 0.3, 0.03 and 0.05 mg m^{-3} in December (Fig. 10). Towards the coast across the NSCS Shelf-sea, TChl_*a* and Fuco increased to over 3 and 0.5 mg m^{-3} respectively in the inner shelf area. Waters with high TChl_*a*, >0.5 mg m^{-3}, were confined to the inner shelf in June, but they covered the entire NSCS north of ~19° N in December. Except in the inner shelf and the Pearl River plume, higher concentrations of TChl_*a* and Fuco were associated with lower SST and vice verse. In contrast, the concentration of Zea did not increase towards the coast. In fact, it seemed to decrease landward in December (Fig. 10). A strip of water with high TChl_*a*, presumably an indication of the river plume, extended from the mouth of the Pearl River southwest-ward along the Chinese coast in both seasons. A corresponding feature was not found in the distribution of SST. Higher TChl_*a* was also found around the Taiwan Bank southwest of Taiwan in both June and December where year-round upwelling has been reported (Hong et al., 2009; Liu et al., 2002; Shang et al., 2004; Tang et al., 2002), northwest of the Luzon Island in December where winter upwelling has been reported (Liu et al., 2002; Shaw et al., 1996; Tang et al., 1999), and around the Dongsha Atoll where internal waves undergo transformation and/or dissipation (Pan et al., 2012; Wang et al., 2007; Zhang et al., 2011; Zhao et al., 2004). The pattern of increasing concentrations of TChl_*a* towards the coasts, the generally higher concentrations of TChl_*a* in the winter relative to the summer, and in association with the Pearl River and known upwelling areas were consistent with previous observations (Gan et al., 2010; Tang et al., 2002; Tseng et al., 2005; Wong et al., 2007) and known oceanographic processes (Hu et al., 2010; Liu et al., 2002; Shaw et al., 1996) and tended to validate the remotely sensed data.

The dominant phytoplankton group transitioned progressively from *Prochlorococcus* to *Synechococcus* and haptophytes and finally to the diatoms across the NSCS Shelf-sea from the open NSCS to the coast (Fig. 10). The transition zone coincided approximately with the area where temperatures below 26–27 °C and TChl_*a* exceeding 0.3–0.5 mg m^{-3} were found. Thus, in December, the transition zone was

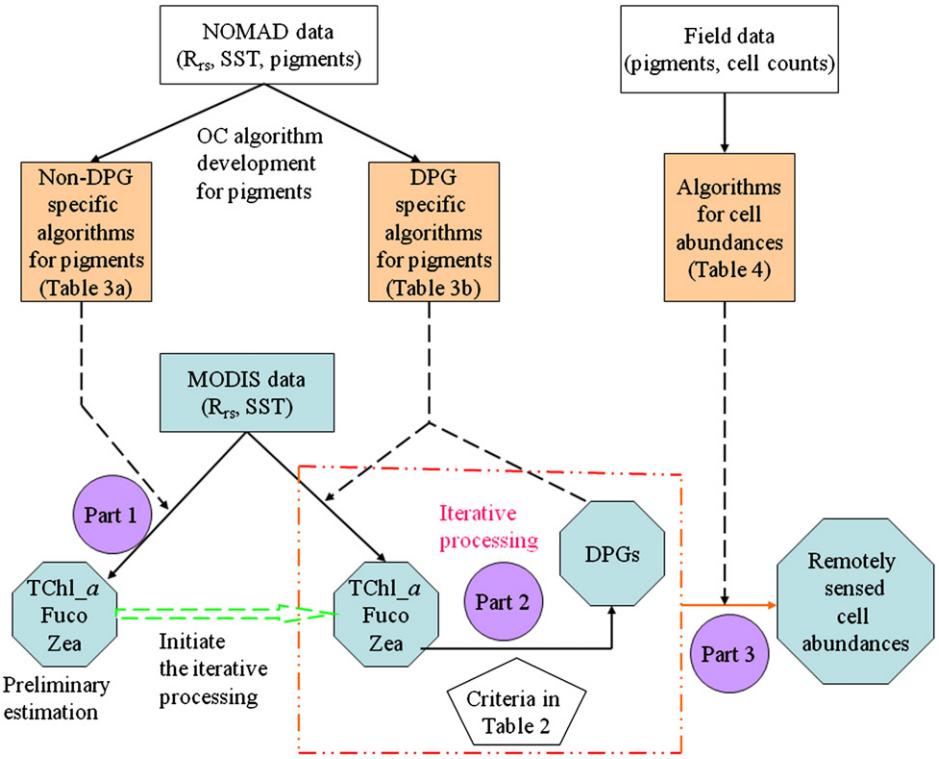

Fig. 8. A flowchart of the scheme for estimating the concentrations of TChl_*a*, Fuco and Zea, the dominant phytoplankton group (DPG) and cell abundance of *Prochlorococcus*, *Synechococcus* and pico-eukaryotes from MODIS data. white and blue rectangles: input data; orange rectangles: empirical algorithms; octagons: output data. OC – Ocean Color; R_{rs} – remote sensing reflectance; SST – sea surface temperature. (For interpretation of the references to color in this figure legend, the reader is referred to the web version of this article.)

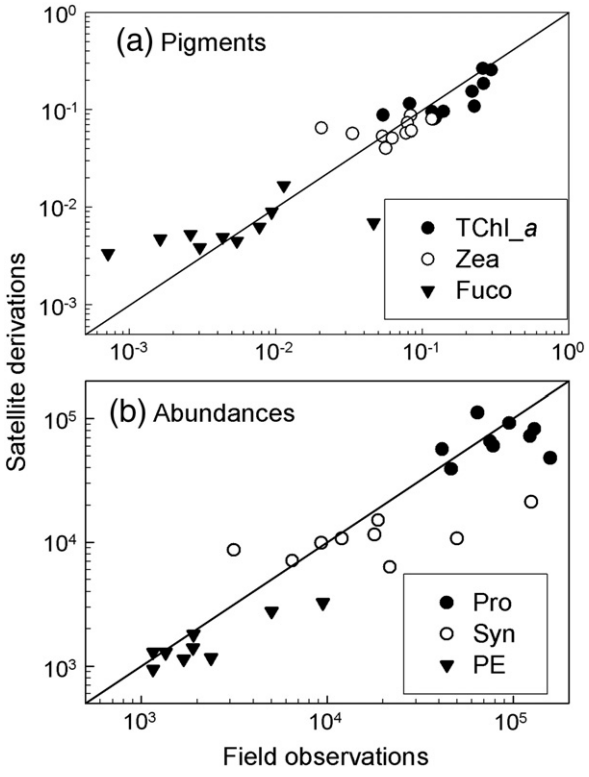

Fig. 9. Relationship between MODIS-Aqua derived and field observed. (a) concentrations (in mg m^{-3}) of TChl_*a*, Zea, and Fuco; and (b) cell abundances (in cells mL^{-1}) of *Prochlorococcus* (Pro), *Synechococcus* (Syn), and pico-eukaryotes (PE). —, 1:1 correspondence.

quite extensive and the dominance of diatoms could be found from around the outer shelf shoreward. On the other hand, in June, the dominance of *Prochlorococcus* extended into the outer and middle shelf, the transition zone was minimal, and the dominance of diatoms was found only in the innermost part of the inner shelf. The dominance of diatoms was also found in the known upwelling areas around the Taiwan Bank year round and northwest of the Luzon Island in December. These patterns were consistent with the expected nutrient conditions in these sub-regions as diatoms were favored under more nutrient-replete conditions while *Prochlorococcus* were favored in nutrient-depleted water (Chen et al., 2004, 2011; Jeffrey et al., 1997; Liu et al., 2007). They were also consistent with those estimated from field samples that were analyzed by HPLC (Fig. 11) and with previous observations (Chen et al., 2007, 2011; Ning et al., 2005). These agreements tended to validate the method proposed here for estimating phytoplankton composition from space.

The corresponding distributions of the cell abundances of *Prochlorococcus*, *Synechococcus* and pico-eukaryotes in June and December 2009 are shown in Fig. 12. In June, across the NSCS Shelf-sea, the abundances of all three picophytoplankton categories increased towards the coast. The abundance of *Prochlorococcus* increased moderately and more gradually from 0.5×10^5 cells mL^{-1} in the open NSCS to 1×10^5 cells mL^{-1} in the inner and middle shelf. On the other hand, the changes

Table 5
Statistical results of the match-up (within ± 48 h) comparisons between the satellite derivations and the field *in situ* measurements.

Parameters	n	MAPD (%)	RMSE
TChl_*a*	13	31.1	0.166
Fuco	10	39.9	0.389
Zea	10	43.0	0.199
N_{Pro}	9	34.8	0.221
N_{Syn}	9	54.5	0.418
N_{PE}	9	28.9	0.220

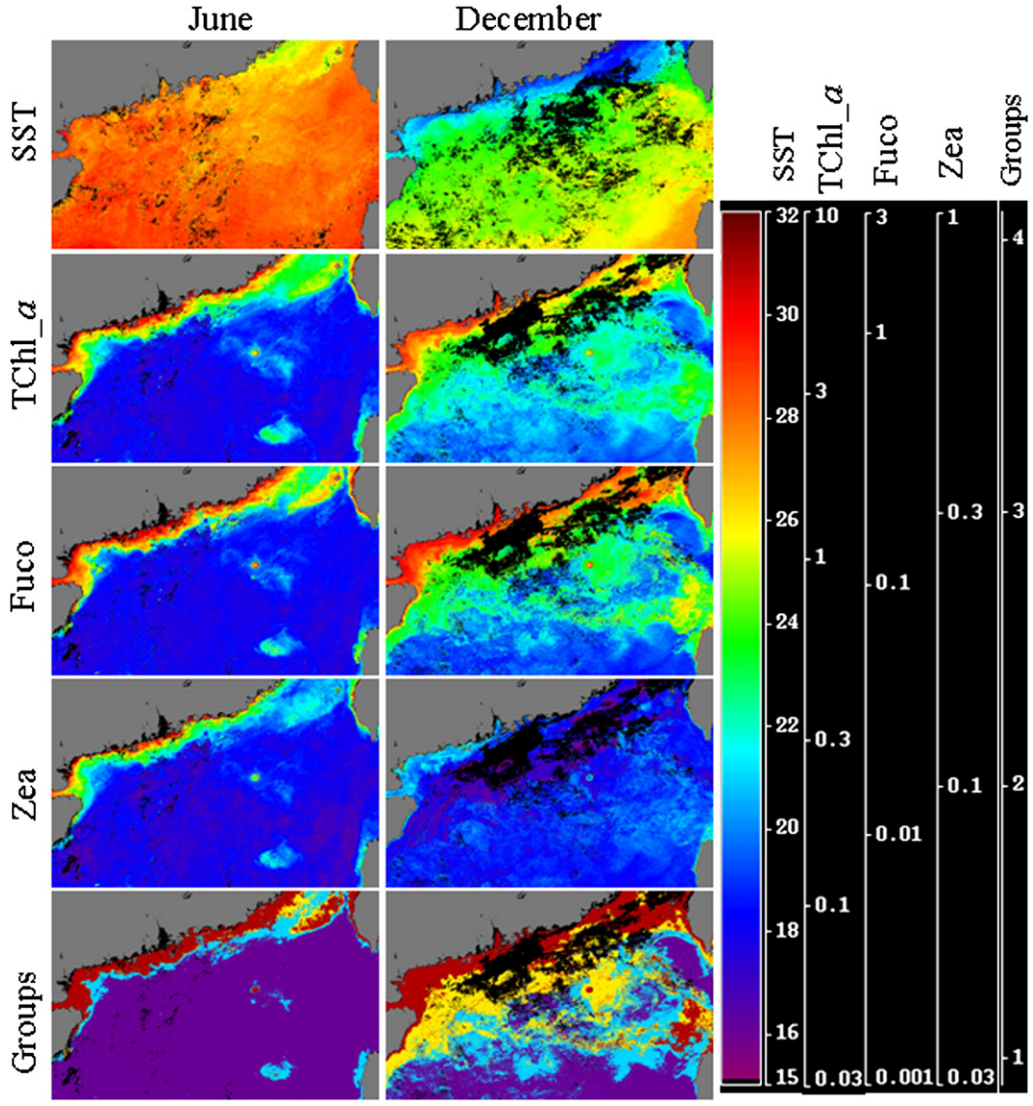

Fig. 10. MODIS-Aqua derived monthly distributions of sea surface temperature (SST; in °C), concentrations (in mg m^{-3}) of TChl_*a*, Fuco, and Zea, and phytoplankton groups in the NSCS in June and December 2009. Groups 1, 2, 3, 4: as defined in Fig. 5. (For interpretation of the references to color in this figure legend, the reader is referred to the web version of this article.)

in the abundances of *Synechococcus* and pico-eukaryotes occurred abruptly between the middle and inner shelf as a narrow strip with elevated abundances, above 1×10^5 and 0.1×10^5 cells mL^{-1} respectively, lined the coast while the corresponding abundances in the open SCS were about an order of magnitude lower. *Prochlorococcus* were clearly the most abundant picophytoplankton in the open NSCS. However, in the inner shelf, the abundance of *Synechococcus* could have become comparable. The pico-eukaryotes were always the least abundant. In December, the abundances of these three picophytoplankton across the NSCS Shelf-sea varied along divergent patterns that could be quite different from those found in June. The abundance of *Prochlorococcus* decreased dramatically from around 1×10^5 cells mL^{-1} in the open NSCS to about 0.1×10^5 cells mL^{-1} in the inner shelf while that of *Synechococcus* increased from 0.1 to 0.3×10^5 cells mL^{-1} in the open NSCS to a maximum of 0.5 to 1×10^5 cells mL^{-1} at the middle shelf before it dropped back to about 0.3×10^5 cells mL^{-1} at the inner shelf. In the meantime, the abundance of pico-eukaryotes increased towards the coast as in June from 0.03×10^5 cells mL^{-1} in the open NSCS to $>0.1\times10^5$ cells mL^{-1} in the inner shelf but the increase was less abrupt. Thus, *Prochlorococcus* were again clearly the most abundant picophytoplankton in the open NSCS as in the June. However, *Synechococcus* became the most abundant in the inner shelf while the pico-eukaryotes remained the least abundant.

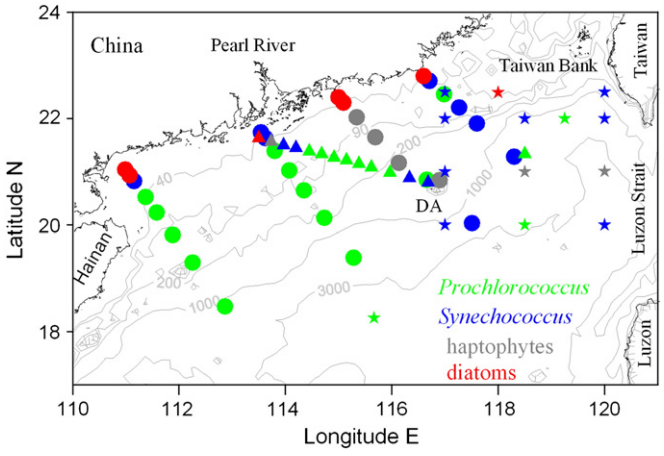

Fig. 11. Dominating phytoplankton groups (*Prochlorococcus*, green symbols; *Synechococcus*, blue symbols; haptophytes, gray symbols; and diatoms, red symbols) in the surface layer of the NSCS in June 2008 (★), June 2009 (▲), and June 2010 (•).(For interpretation of the references to color in this figure legend, the reader is referred to the web version of this article.)

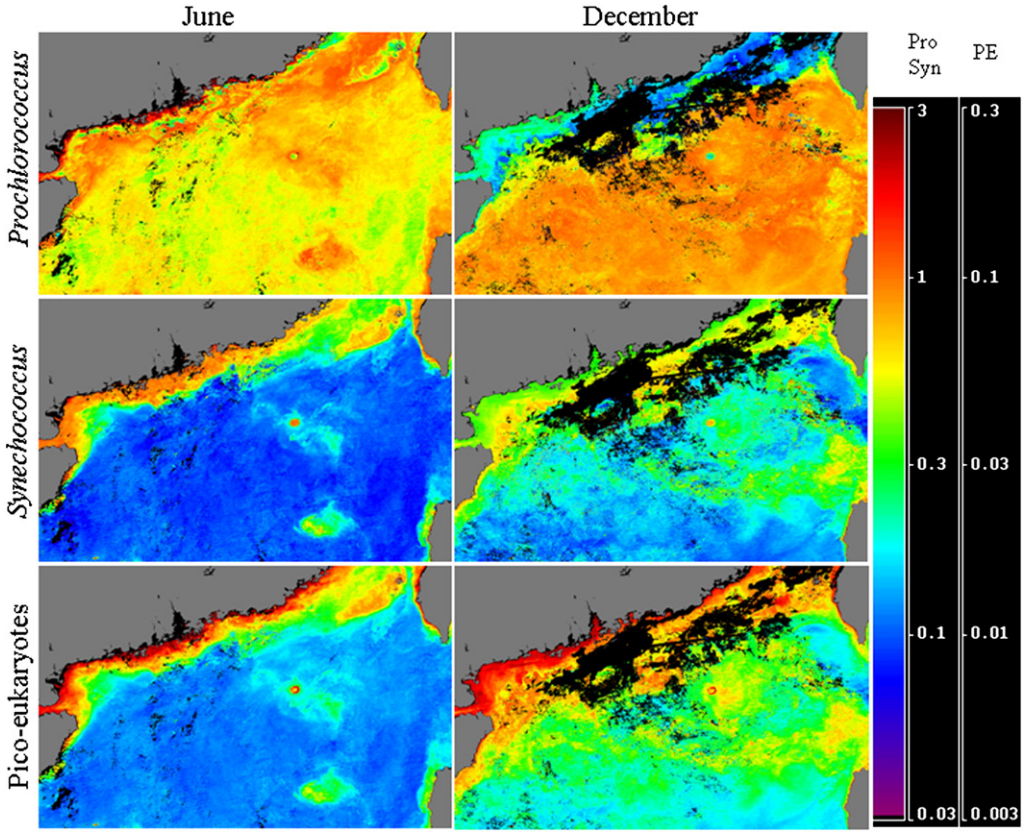

Fig. 12. MODIS-Aqua derived monthly distributions of the cell abundances (in 10^5 cells mL^{-1}) of *Prochlorococcus*, *Synechococcus*, and pico-eukaryotes in the NSCS in June and December 2009. (For interpretation of the references to color in this figure legend, the reader is referred to the web version of this article.)

Relative to June, the total abundance of all three picophytoplankton categories became notably elevated in the open NSCS and in most of the NSCS Shelf-sea.

The sensitivities of these distributional patterns derived from remote sensing to the statistical errors in the empirical relationships were tested by allowing the log-transformed concentrations of the accessory pigments to vary by plus or minus one RMSE as determined in the comparison between *in situ* observations and remotely sensed data (Table 5) and then re-calculating the corresponding concentrations of the pigments, phytoplankton composition and cell abundances. The results, given in Figs. S2 and S3 in the auxiliary material, indicated that the general patterns across the shelf and in the NSCS stayed unchanged. Thus, at least the qualitative conclusions that were drawn from the remotely sensed data were not materially affected by these statistical uncertainties.

3.6.2. Time-series distributions at SEATS and the inner shelf of the NSCS Shelf-sea

The monthly means in SST, TChl_*a*, phytoplankton groups, and cell abundances of picophytoplankton, all derived from MODIS-Aqua data, at the location of the anchored station in the inner shelf at the vicinity of the mouth of the Pearl River and at the SEATS station (Fig. 1) from 2002 to 2011 are shown in Fig. 13. Variations in SST followed the same pattern and the summer temperatures were similar at both stations (Fig. 13a). However, the amplitude in the inner shelf, about 13 °C, was about twice of that at the SEATS station (Fig. 13a). At the SEATS station, the concentrations of TChl_*a* were mostly below 0.2 mg m^{-3}, as reported previously (Pan et al., 2012; Tseng et al., 2005), and a winter maximum was invariably found. The dominant phytoplankton group was mostly *Prochlorococcus*. Occasionally, *Synechococcus* could become dominant and this occurred almost invariably around the winter. The cell abundance decreased in the order of *Prochlorococcus* to *Synechococcus* to pico-eukaryotes. The intra-annual variations in the cell abundances were the smallest in *Synechococcus*. The variations were more conspicuous in *Prochlorococcus* but they did not follow clear seasonal patterns. On the other hand, a winter maximum was found in the pico-eukaryotes. In the inner shelf, intra-annual variations generally became more prominent. The concentrations of TChl_*a* were mostly above 0.5 mg m^{-3} but the intra-annual variations did not follow a clear seasonal pattern. The dominant phytoplankton group was more variable than at SEATS. In most cases, the diatoms were the dominant but *Synechococcus* frequently became dominant in the late spring and summer. Haptophytes became dominant infrequently while *Prochlorococcus* almost never became dominant. The cell abundance of *Synechococcus* was usually the highest throughout the year. Its intra-annual variations were small and they did not follow a definitive seasonal pattern. In contrast, the cell abundance of *Prochlorococcus* fluctuated conspicuously and reached a maximum in the summer and a minimum in the winter. The abundance of the pico-eukaryotes also varied intra-annually but there was no clear seasonal pattern. In comparison to those at the SEATS station, the cell abundance of both *Synechococcus* and the pico-eukaryotes were about an order of magnitude higher in the inner shelf. For *Prochlorococcus*, while there were significant seasonal fluctuations, the annual average abundance in the inner shelf was similar to that at the SEATS station. Again, these time-series observations were consistent with previous observations (Chen & Chen, 2006; Chen et al., 2011; Gan et al., 2010; Liu et al., 2007; Tseng et al., 2005), and thus tended to validate our approach for the remote sensing data.

4. Summary

This paper demonstrated a method for assessing the distributional patterns of picophytoplankton and their cell abundances from remote sensing. The method was based on the development of improved algorithms (1) for estimating the concentrations of fucoxanthin and zeaxanthin from MODIS data; (2) for identifying the dominant phytoplankton

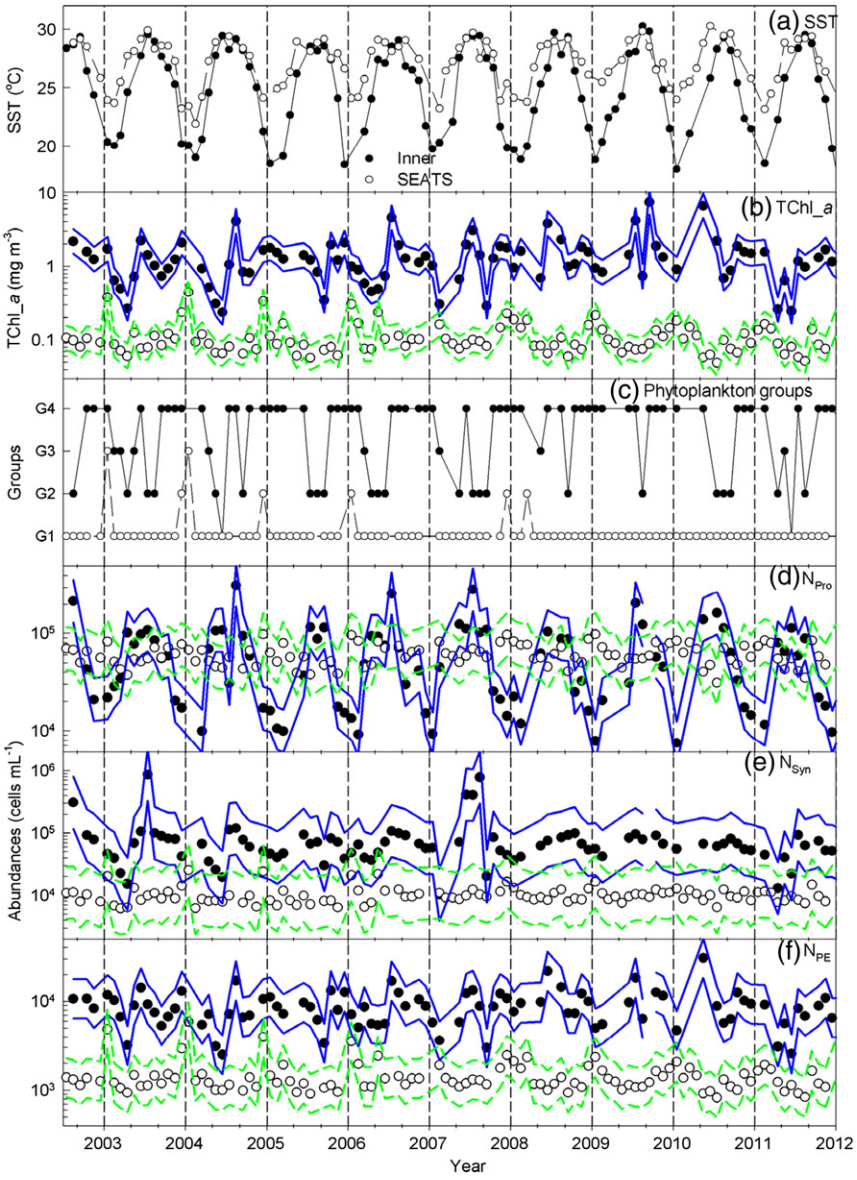

Fig. 13. MODIS-Aqua derived monthly (a) SST, (b) TChl_*a*, (c) dominant phytoplankton groups (G1, G2, G3, G4: defined as in Fig. 5), and cell abundances of (d) *Prochlorococcus* (N_{Pro}), (e) *Synechococcus* (N_{Syn}) and (f) pico-eukaryotes (N_{PE}) in the inner-shelf at 21.63° N, 113.50° E (●) and in the open SCS at 18.00° N, 116.00° E (SEATS station; o). — and ---- in (b), (d), (e) and (f): uncertainty based on RMSE in inner shelf and open SCS data. (For interpretation of the references to color in this figure legend, the reader is referred to the web version of this article.)

group among *Prochlorococcus*, *Synechococcus*, haptophytes and diatoms, the four primary phytoplankton groups in the world's oceans, from the concentrations of total chlorophyll *a* and these two accessory pigments; and (3) for relating the cell abundances of *Prochlorococcus*, *Synechococcus*, and pico-eukaryotes to the concentrations of these pigments. The distributional patterns of the phytoplankton groups in the NSCS and especially the NSCS Shelf-sea were examined by using this method. The resulting general patterns were consistent with the known oceanography of the region in terms of both phytoplankton composition and cell abundances. Thus, the dominant phytoplankton group transitioned from the *Prochlorococcus* to *Synechococcus* to the haptophytes to the diatoms from the open SCS to inner shelf. In terms of cell abundance, *Prochlorococcus* were most abundant in the open SCS while *Synechococcus* could become the most abundant in the inner shelf. The pico-eukaryotes were invariably the least abundant. However, its abundance did increase towards the coast. These general agreements between the remotely sensed and expected patterns tended to validate the method proposed here. In addition, other processes that might affect the distribution of the phytoplankton in the NSCS, namely the effects of internal waves off the Dongsha Atoll, riverine discharge off the mouth of the Pearl River, upwelling off the Taiwan Bank and winter upwelling off Luzon Island were also captured reasonably well in the patterns derived from the remotely sensed products. This work represents the first effort in assessing the abundances of the principal picophytoplankton in the ocean from remotely sensed data. Since some of the algorithms developed in this study were established by using *in situ* observations from the NSCS only, the application of this approach to other parts of the ocean will require further testing by using data beyond this region.

Acknowledgements

We are grateful to Kuo-Yuan Li and Hsu-Han Yang for their determination of nutrients and pigment concentrations in water samples, to the participants in the SouthEast Asian Time-series Study (SEATS) for making their archive data available, to Xianghui Guo for providing the Pearl River discharge data, and to the captains and the crews of R/V *Ocean Researcher I* and *Ocean Researcher III* for their assistance in sample collection. We also thank the participants for making their archive data available to the

NOMAD dataset, and J. Werdell for compiling these data. This work was supported in part by the National Science Council, Taiwan through grants NSC98-2611-M-001-004-MY3 and NSC100-2611-M-001-001 (to Wong) and NSC99-2811-M-001-093, NSC100-2811-M-001-095, and NSC101-2811-M-001-083 (to Pan), and by the Academia Sinica through the grants titled "Atmospheric Forcing on Ocean Biogeochemistry (AFOBi)" and "Ocean Acidification: Comparative biogeochemistry in shallow-water tropical coral reef ecosystems in a naturally acidic marine environment" (to Wong). The remarks from two anonymous reviewers were extremely helpful and significantly improved the paper.

Appendix A. Supplementary data

Supplementary data to this article can be found online at http://dx.doi.org/10.1016/j.rse.2012.10.014.

References

Agawin, N. S. R., Duarte, C. M., Agusti, S., & McManus, L. (2003). Abundance, biomass and growth rates of *Synechococcus* sp. in a tropical coastal ecosystem (Philippines, South China Sea). *Estuarine, Coastal and Shelf Science*, *56*, 493–502.

Aiken, J., Hardman-Mountford, N. J., Barlow, R., Fishwick, J., Hirata, T., & Smyth, T. (2008). Functional links between bioenergetics and bio-optical traits of phytoplankton taxonomic groups: an overreaching hytpothesis with application for ocean colour remote sensing. *Journal of Plankton Research*, *30*, 165–181.

Alvain, S., Moulin, C., Dandonneau, Y., & Breon, F. M. (2005). Remote sensing of phytoplankton groups in case 1 waters from global SeaWiFS imagery. *Deep-Sea Research I*, *52*, 1989–2004.

Bailey, S. W., & Werdell, P. J. (2006). A multi-sensor approach for the on-orbit validation of ocean color satellite data products. *Remote Sensing of Environment*, *102*, 12–23.

Bidigare, R. R., Van Heukelem, L., & Trees, C. C. (2002). HPLC phytoplankton pigments: sampling, laboratory methods, and quality assurance procedures. In J. L. Mueller, & G. S. Fargion (Eds.), *Ocean optics protocols for satellite ocean color sensor validation, Revision 3, Vol. 2*, Greenbelt, Maryland: NASA Goddard Space Flight Center (NASA/TM-2002-210001/Rev3-Vol2).

Bricaud, A., Claustre, H., Ras, J., & Oubelkheir, K. (2004). Natural variability of phytoplanktonic absorption in oceanic waters: Influence of the size structure of algal populations. *Journal of Geophysical Research*, *109*, C11010, http://dx.doi.org/10.1029/2004JC002419.

Campbell, L., Nolla, H. A., & Vaulot, D. (1994). The importance of *Prochlorococcus* to community structure in the central North Pacific Ocean. *Limnology and Oceanography*, *39*, 954–961.

Campbell, L., & Vaulot, D. (1993). Photosynthetic picoplankton community structure in the subtropical North Pacific Ocean near Hawaii (station ALOHA). *Deep-Sea Research I*, *40*(10), 2043–2060.

Chen, Y. L., & Chen, H. -Y. (2006). Seasonal dynamics of primary and new production in the northern South China Sea: The significance of river discharge and nutrient advection. *Deep-Sea Research I*, *53*(6), 971–986.

Chen, Y. L., Chen, H. -Y., & Chung, C. -W. (2007). Seasonal variability of coccolithophore abundance and assemblages in the northern South China Sea. *Deep-Sea Research II*, *54*, 1617–1633.

Chen, Y. L. L., Chen, H. Y., Karl, D. M., & Takahashi, M. (2004). Nitrogen modulates phytoplankton growth in spring in the South China Sea. *Continental Shelf Research*, *24*, 527–541, http://dx.doi.org/10.1016/j.csr.2003.12.006.

Chen, C. -C., Shiah, F. -K., Chung, S. -W., & Liu, K. -K. (2006). Winter phytoplankton blooms in the shallow mixed layer of the South China Sea enhanced by upwelling. *Journal of Marine Systems*, *59*, 97–110.

Chen, B., Wang, L., Song, S., Huang, B., Sun, J., & Liu, H. (2011). Comparisons of picophytoplankton abundance, size, and fluorescence between summer and winter in northern South China Sea. *Continental Shelf Research*, *31*, 1527–1540, http://dx.doi.org/10.1016/j.csr.2011.06.018.

Chisholm, S. W. (1992). Phytoplankton size. In P. G. Falkowski, & A. D. Woodhead (Eds.), *Primary productivity and biogeochemical cycles in the sea* (pp. 213–237). New York: Plenum Press.

Claustre, H., Bricaud, A., Babin, M., Bruyant, F., Guillou, L., Gall, F. L., et al. (2002). Diel variations in Prochlorococcus optical properties. *Limnology and Oceanography*, *47*(6), 1637–1647.

Claustre, H., Hooker, S. B., Van Heukelemc, L., Berthon, J. -F., Barlow, R., Ras, J., et al. (2004). An intercomparison of HPLC phytoplankton pigment methods using *in situ* samples: Application to remote sensing and database activities. *Marine Chemistry*, *85*, 41–61.

Dai, M., Zhai, W., Cai, W. -J., Callahan, J., Huang, B., Shang, S., et al. (2008). Effects of an estuarine plume-associated bloom on the carbonate system in the lower reaches of the Pearl River estuary and the coastal zone of the northern South China Sea. *Continental Shelf Research*, *28*, 1416–1423.

Gan, J., Cheung, A., Guo, X., & Li, L. (2009a). Intensified upwelling over a widened shelf in the northeastern South China Sea. *Journal of Geophysical Research*, *114*, C09019, http://dx.doi.org/10.1029/2007JC004660.

Gan, J., Li, L., Wang, D., & Guo, X. (2009b). Interaction of a river plume with coastal upwelling in the northeastern South China Sea. *Continental Shelf Research*, *29*, 728–740.

Gan, J., Lu, Z., Dai, M., Cheung, A. Y. Y., Liu, H., & Harrison, P. (2010). Biological response to intensified upwelling and to a river plume in the northeastern South China Sea: A modeling study. *Journal of Geophysical Research*, *115*, C09001, http://dx.doi.org/10.1029/2009JC005569.

Hirata, T., Hardman-Mountford, N. J., Brewin, R. J. W., Aiken, J., Barlow, R., Suzuki, K., et al. (2011). Synoptic relationships between surface Chlorophyll-*a* and diagnostic pigments specific to phytoplankton functional types. *Biogeosciences*, *8*, 311–327, http://dx.doi.org/10.5194/bg-8-311-2011.

Hong, H., Zhang, C., Shang, S., Huang, B., Li, Y., Li, X., et al. (2009). Interannual variability of summer coastal upwelling in the Taiwan Strait. *Continental Shelf Research*, *29*, 479–484.

Hu, J. Y., Kawamura, H., Li, C. Y., Hong, H. S., & Jiang, Y. W. (2010). Review on current and seawater volume transport through the Taiwan Strait. *Journal of Oceanography*, *66*(5), 591–610.

International Ocean-Colour Coordinating Group (IOCCG) (2006). Remote sensing of inherent optical properties: Fundamentals, tests of algorithms, and applications. In Z. -P. Lee (Ed.), *Reports of the International Ocean-Colour Coordinating Group, no. 5*, Dartmouth, Canada: IOCCG.

Jeffrey, S. W., Mantoura, R. F. C., & Wright, S. W. (1997). *Phytoplankton pigments in oceanography*. Paris: UNESCO Publishing.

Kuster, T., Metsamaa, L., Strombeck, N., & Vahtmae, E. (2006). Monitoring cyanobacterial blooms by satellite remote sensing. *Estuarine, Coastal and Shelf Science*, *67*, 303–312.

Li, W. K. W., Rao, D. V. S., Harrison, W. G., Smith, J. C., Cullen, J. J., Irwin, B., et al. (1983). Autotrophic picoplankton in the tropical ocean. *Science*, *219*, 292–295.

Lin, I. -I., Hu, C., Li, Y. -H., Ho, T. -Y., Wong, G. T. F., Wu, J., et al. (2011). Fertilization potential of volcanic dust in the low-nutrient low-chlorophyll western North Pacific subtropical gyre: Satellite evidence and laboratory study. *Global Biogeochemical Cycles*, *25*, GB1006, http://dx.doi.org/10.1029/2009GB003758.

Lin, I. -I., Lien, C. -C., Wu, C. -R., Wong, G. T. F., Huang, C. -W., & Chiang, T. -L. (2010). Enhanced primary production in the oligotrophic South China Sea by eddy injection in spring. *Geophysical Research Letters*, *37*, L16602, http://dx.doi.org/10.1029/2010GL043872.

Lin, I., Liu, W. T., Wu, C. -C., Wong, G. T. F., Hu, C., Chen, Z., et al. (2003). New evidence for enhanced ocean primary production triggered by tropical cyclone. *Geophysical Research Letters*, *30*(13), 1718, http://dx.doi.org/10.1029/2003GL017141.

Liu, H., Chang, J., Tseng, C. -M., Wen, L. -S., & Liu, K. K. (2007). Seasonal variability of picoplankton in the Northern South China Sea at the SEATS station. *Deep-Sea Research II*, *54*, 1602–1616.

Liu, K. K., Chao, S. Y., Shaw, P. T., Gong, G. C., Chen, C. C., & Tang, T. Y. (2002). Monsoon-forced chlorophyll distribution and primary production in the South China Sea: Observations and a numerical study. *Deep-Sea Research I*, *49*, 1387–1412.

Liu, C. -T., Pinkel, R., Hsu, M. -K., Klymak, J. M., Chien, H. -W., & Villanoy, C. (2006). Nonlinear internal waves from the Luzon Strait. *EOS. Transactions of the American Geophysical Union*, *87*(42), 449–451.

Mills, M. M., Ridame, C., Davey, M., La Roche, J., & Geider, R. J. (2004). Iron and phosphorus co-limit nitrogen fixation in the eastern tropical North Atlantic. *Nature*, *429*, 292–294, http://dx.doi.org/10.1038/nature02550.

Mobley, C. (1994). *Light and water: Radiative transfer in natural waters*. San Diego: Academic Press.

Ning, X., Li, W. K. W., Cai, Y., & Shi, J. (2005). Comparative analysis of bacterioplankton and phytoplankton in three ecological provinces of the northern South China Sea. *Marine Ecology Progress Series*, *293*, 17–28.

O'Reilly, J. E., Maritorena, S., Mitchell, B. G., Siegel, D. A., Carder, K. L., Garver, S. A., et al. (1998). Ocean color algorithms for SeaWiFS. *Journal of Geophysical Research*, *103*, 24937–24953.

Pan, X., Mannino, A., Marshall, H. G., Filippino, K. C., & Mulholland, M. R. (2011). Remote sensing of phytoplankton community composition along the northeast coast of the United States. *Remote Sensing of Environment*, *115*, 3731–3747, http://dx.doi.org/10.1016/j.rse.2011.09.011.

Pan, X., Mannino, A., Russ, M. E., & Hooker, S. B. (2008). Remote sensing of the absorption coefficients and chlorophyll a concentration in the United States southern Middle Atlantic Bight from SeaWiFS and MODIS-Aqua. *Journal of Geophysical Research*, *113*, C11022, http://dx.doi.org/10.1029/2008JC004852.

Pan, X., Mannino, A., Russ, M. E., Hooker, S. B., & Harding, L. W. (2010). Remote sensing of phytoplankton pigment distribution in the United States northeast coast. *Remote Sensing of Environment*, *114*, 2403–2416, http://dx.doi.org/10.1016/j.rse.2010.05.015.

Pan, X., Wong, G. T. F., Shiah, F. -K., & Ho, T. -Y. (2012). Enhancement of biological productivity by internal waves: Observations in the summertime in the northern South China Sea. *Journal of Oceanography*, *68*, 427–437, http://dx.doi.org/10.1007/s10872-012-0107-y.

Qiu, D., Huang, L., Zhang, J., & Lin, S. (2010). Phytoplankton dynamics in and near the highly eutrophic Pearl River Estuary, South China Sea. *Continental Shelf Research*, *30*, 177–186.

Randolph, K., Wilson, J., Tedesco, L., Li, L., Pascual, D. L., & Soyeux, E. (2008). Hyperspectral remote sensing of cyanobacteria in turbid productive water using optically active pigments, chlorophyll a and phycocyanin. *Remote Sensing of Environment*, *112*, 4009–4019.

Ruiz-Verdú, A., Simis, S. G. H., Hoyos, C., Gons, H. J., & Peña-Martínez, R. (2008). An evaluation of algorithms for the remote sensing of cyanobacterial biomass. *Remote Sensing of Environment*, *112*, 3996–4008.

Shang, S. L., Zhang, C. Y., Hong, H. S., Shang, S. P., & Chai, F. (2004). Short-term variability of chlorophyll associatedwith upwelling events in the Taiwan Strait during the southwest monsoon of 1998. *Deep-Sea Research II*, *51*, 1113–1127, http://dx.doi.org/10.1016/j.dsr2.2004.04.003.

Shaw, P. -T. (1989). The intrusion of water types into the sea southwest of Taiwan. *Journal of Geophysical Research*, *94*(C12), 18213–18226.

Shaw, P. -T., & Chao, S. -Y. (1994). Surface circulation in the South China Sea. *Deep-Sea Research I*, *41*, 1663–1683.

Shaw, P. -T., Chao, S. -Y., Liu, K. -K., Pai, S. -C., & Liu, C. -T. (1996). Winter upwelling off Luzon in the northeastern South China Sea. *Journal of Geophysical Research*, *101*(C7), 16435–16448.

Shiozaki, T., Furuya, K., Kodama, T., Kitajima, S., Takeda, S., Takemura, T., et al. (2010). New estimation of N_2 fixation in the western and central Pacific Ocean and its marginal seas. *Global Biogeochemical Cycles*, *24*, GB1015, http://dx.doi.org/10.1029/2009GB003620.

Tang, D. L., Kawamura, H., Shi, P., Takahashi, W., Guan, L., Shimada, T., et al. (2006). Seasonal phytoplankton blooms associated with monsoonal influences and coastal environments in the sea areas either side of the Indochina Peninsula. *Journal of Geophysical Research*, *111*, G01010, http://dx.doi.org/10.1029/2005JG000050.

Tang, D. L., Kester, D. R., Ni, I. -H., Kawamura, H., & Hong, H. (2002). Upwelling in the Taiwan Strait during the summer monsoon detected by satellite and shipboard measurements. *Remote Sensing of Environment*, *83*, 457–471.

Tang, D. L., Ni, I. -H., Kester, D. R., & Müller-Karger, F. E. (1999). Remote sensing observation of winter phytoplankton blooms southwest of the Luzon Strait in the South China Sea. *Marine Ecology Progress Series*, *191*, 43–51.

Tseng, C. -M., Wong, G. T. F., Lin, I. -I., Wu, C. -R., & Liu, K. -K. (2005). A unique seasonal pattern in phytoplankton biomass in low-latitude waters in the South China Sea. *Geophysical Research Letters*, *32*, L08608, http://dx.doi.org/10.1029/2004GL022111.

Uitz, J., Claustre, H., Morel, A., & Hooker, S. B. (2006). Vertical distribution of phytoplankton communities in open ocean: An assessment based on surface chlorophyll. *Journal of Geophysical Research*, *111*, C08005, http://dx.doi.org/10.1029/2005JC003207.

Vaulot, D., Eikrem, W., Viprey, M., & Moreau, H. (2008). The diversity of small eukaryotic phytoplankton ($\leq$3 μm) in marine ecosystems. *FNMS Microbiology Reviews*, *32*(5), 795–820, http://dx.doi.org/10.1111/j.1574-6976.2008.00121.x.

Wang, Y. -H., Dai, C. -F., & Chen, Y. -Y. (2007). Physical and ecological processes of internal waves on an isolated reef ecosystem in the South China Sea. *Geophysical Research Letters*, *34*, L18609, http://dx.doi.org/10.1029/2007GL030658.

Werdell, P. J., & Bailey, S. W. (2005). An improved bio-optical data set for ocean color algorithm development and satellite data product validation. *Remote Sensing of Environment*, *98*(1), 122–140.

Wong, G. T. F., Tseng, C. -M., Wen, L. -S., & Chung, S. -W. (2007). Nutrient dynamics and N-anomaly at the SEATS station. *Deep-Sea Research II*, *54*, 1528–1545, http://dx.doi.org/10.1016/j.dsr2.2007.05.011.

Wu, J., Chung, S. -W., Wen, L. -S., Liu, K. -K., Chen, Y. L. L., Chen, H. -Y., et al. (2003). Dissolved inorganic phosphorus, dissolved iron, and *Trichodesmium* in the oligotrophic South China Sea. *Global Biogeochemical Cycles*, *17*(1), 1008, http://dx.doi.org/10.1029/2002GB001924.

Yin, K. (2002). Monsoonal influence on seasonal variations in nutrients and phytoplankton biomass in coastal waters of Hong Kong in the vicinity of the Pearl River estuary. *Marine Ecology Progress Series*, *245*, 111–122.

Zhang, Z., Fringer, O. B., & Ramp, S. R. (2011). Three dimensional, nonhydrostatic numerical simulation of nonlinear internal wave generation and propagation in the South China Sea. *Journal of Geophysical Research*, *116*, C05022, http://dx.doi.org/10.1029/2010JC006424.

Zhao, Z., Klemas, V., Zheng, Q., & Yan, X. -H. (2004). Remote sensing evidence for baroclinic tide origin of internal solitary waves in the northeastern South China Sea. *Geophysical Research Letters*, *31*, L06302, http://dx.doi.org/10.1029/2003GL019077.